Commun Nonlinear Sci Numer Simulat 22 (2015) 1201–1214

Contents lists available at ScienceDirect

Commun Nonlinear Sci Numer Simulat

journal homepage: www.elsevier.com/locate/cnsns

Calculation of homoclinic and heteroclinic orbits in 1D maps

Viktor Avrutin [a,c,*], Björn Schenke [b], Laura Gardini [c]

[a] IST, University of Stuttgart, Germany
[b] IPVS, University of Stuttgart, Germany
[c] DESP, University of Urbino, Italy

ARTICLE INFO

Article history:
Received 18 February 2014
Received in revised form 23 June 2014
Accepted 7 July 2014
Available online 1 August 2014

Keywords:
Homoclinic orbits
Heteroclinic connections
Algorithms
Homoclinic and heteroclinic bifurcations
Piecewise smooth maps
Discontinuous maps
Chaotic attractors

ABSTRACT

Homoclinic orbits and heteroclinic connections are important in several contexts, in particular for a proof of the existence of chaos and for the description of bifurcations of chaotic attractors. In this work we discuss an algorithm for their numerical detection in smooth or piecewise smooth, continuous or discontinuous maps. The algorithm is based on the convergence of orbits in backward time and is therefore applicable to expanding fixed points and cycles. For simplicity, we present the algorithm using 1D maps.

1. Introduction

When dealing with chaotic sets (chaotic attractors or repellers), the concept of homoclinic orbits and heteroclinic connections plays a central role. In particular, it can be used for the proof of the existence of chaos. Indeed, it is proved in [12,6,13] that the existence of a non-degenerate (persistent under parameter perturbation) homoclinic orbit to an expanding fixed point of a smooth map f implies the existence of an invariant set in a neighborhood of the homoclinic orbit, on which f is chaotic. Note that the same result applies also for a non-degenerate heteroclinic connection. For piecewise smooth (continuous and discontinuous) maps this result was extended in [8], where the concept of a critical homoclinic orbit was introduced. Recall that in the framework of homoclinic orbits and heteroclinic connections, for a continuous function f the only points we call critical points are fold points (that is, for 1D maps, the values at smooth or non-smooth local extrema), while for discontinuous piecewise smooth functions also the values at discontinuity points are called critical points. A homoclinic orbit or a heteroclinic connection which includes a critical point is called critical and is non-persistent under parameter perturbations. It was proved that the existence of a non-critical homoclinic orbit implies the existence of chaos in its neighborhood, a similar result applies also for non-critical heteroclinic connections.

Investigating homoclinic orbits and heteroclinic connections is relevant not only for the proof of the existence of chaos but also for the description of several bifurcations of chaotic attractors (crisis bifurcations), since such bifurcations are caused by homoclinic bifurcations of repelling fixed points or cycles. This issue is of a particular interest when dealing with piecewise smooth systems (continuous or discontinuous), as these are able to show chaotic dynamics in extended regions in

* Corresponding author at: IST, University of Stuttgart, Germany.
E-mail addresses: Viktor.Avrutin@ist.uni-stuttgart.de (V. Avrutin), Bjoern.Schenke@ipvs.uni-stuttgart.de (B. Schenke), Laura.Gardini@uniurb.it (L. Gardini).

http://dx.doi.org/10.1016/j.cnsns.2014.07.008
1007-5704/

the parameter space (following [5], denoted as robust chaos). The domain of robust chaos may be organized in complex bifurcation scenarios [3,4,1] formed by several bifurcations of chaotic attractors, frequently referred to as crises [10,11,9] or contact bifurcations [15,7,14]. Such bifurcations may lead to a sudden change of the shape of the attractor, or to a change of the number of its bands (connected components), and are necessarily related to a homoclinic bifurcation of a repelling cycle. Moreover, it is proved in [8] that they are associated with the existence of a critical homoclinic orbit. Due to the presence of a critical homoclinic orbit at the bifurcation point, the properties of the cycle undergoing the homoclinic bifurcation may change. In particular, it can be non-homoclinic before the bifurcation and homoclinic after. For example this occurs in the case of a merging bifurcation, at which some bands of a multi-band chaotic attractor merge pairwise [2]. It can also be non-homoclinic before the bifurcation and one-side homoclinic after. This happens for example in the case of a final bifurcation (boundary crisis) in a 1D map, at which a chaotic attractor is transformed into a chaotic repeller [2]. Therefore, to describe such bifurcations it is necessary to determine the properties of the involved cycles, in particular whether they are homoclinic or not.

To determine if there exists a homoclinic orbit to a particular cycle or a heteroclinic connection between two particular cycles of interest, it is necessary to analyze the global structure of the phase space. In most of the cases, this can only be done numerically. The goal of this paper is to discuss an algorithm for the detection of homoclinic orbits and heteroclinic connections. By contrast to algorithms related to local stable and unstable manifolds of saddles, the algorithm discussed below is based on convergence of orbits in backward time and hence it is applicable to expanding fixed points and cycles. In the present work we discuss the algorithm only for 1D maps, in which case every repelling fixed point or cycle is expanding.

The paper is organized as follows. In Section 2 we collect the basic definitions regarding homoclinic orbits and heteroclinic connections. In Section 3 we show the basic idea of the algorithm for finding homoclinic orbits and heteroclinic connections to repelling fixed points in 1D maps. Technical issues regarding possible implementations of the algorithm are discussed in Section 4. Thereafter, in Section 5 we discuss possible problems that appear when the algorithm is applied to the detection of homoclinic orbits and heteroclinic connections to repelling cycles, as well as the solutions of these problems. In Section 6 some examples are shown. To conclude, in Section 7 we discuss a possible extension of the algorithm to higher-dimensional systems.

2. Definitions and properties

Let us first recall some basic definitions and notions. In the following we consider a 1D map defined by a function f which may be smooth or piecewise smooth, continuous or discontinuous. We assume f to be piecewise monotone:

$$x_{n+1} = f(x_n) = \begin{cases} f_1(x_n) & \text{if } x_n \in \mathcal{D}_1 \\ \dots & \\ f_k(x_n) & \text{if } x_n \in \mathcal{D}_k \end{cases} \tag{1}$$

where $\mathcal{D}_j,\ j = 1,\dots,k$ are (bounded or at most one-side unbounded) intervals of monotonicity of f. Accordingly, each function f_j is invertible on its domain $\mathcal{D}_j,\ j = 1,\dots,k$, i.e. there exists an inverse function

$$f_j^{-1} : \mathcal{V}_j \mapsto \mathcal{D}_j \quad \text{with } \mathcal{V}_j = f(\mathcal{D}_j) \tag{2}$$

The border points of the intervals $\mathcal{D}_j$ are the points at which the derivative f' is either equal to zero (smooth extrema of f) or not defined (kink points and discontinuity points of f). We assume further that map (1) has an invariant interval $\mathcal{I}$, i.e. $f(\mathcal{I}) = \mathcal{I}$.

Let us consider now a repelling fixed point $x^* \in \mathcal{I}$ of map (1). For sake of simplicity, we assume that f is smooth in x^* (although the results remain correct also for the case that f is non-smooth but continuous in x^*) and that x^* belongs to the interior of some interval of monotonicity, denoted in the following by $\mathcal{D}_\ell$, $\ell \in \{1,\dots,k\}$. Recall that the stable and unstable sets of x^* are defined by

$$\mathbb{W}^s(x^*) = \left\{ x \mid \lim_{i\to\infty} f^i(x) = x^* \right\} \tag{3}$$

$$\mathbb{W}^u(x^*) = \left\{ x \mid \lim_{i\to\infty} f_{j_i}^{-i}(x) = x^* \right\} \tag{4}$$

Note that $\{f_{j_i}^{-i}(x)\}_{i=0}^{i=\infty}$ represents a suitable sequence of preimages, that leads from the point x to the fixed point x^*, with $j_i \in \{1,\dots,k\}$. In other words, the stable set $\mathbb{W}^s(x^*)$ of x^* is the set of points x for which x^* is the ω-limit set and the unstable set $\mathbb{W}^u(x^*)$ of x^* is the set of points x for which x^* is the α-limit set. As we assume x^* to be repelling on both sides, the set $\mathbb{W}^s(x^*)$ consists of points which are eventually mapped on x^*, i.e. the set of preimages of x^* of all ranks. In this case, Eq. (3) is equivalent to

$$\mathbb{W}^s(x^*) = \left\{ x \mid f^{n_x}(x) = x^*,\ n_x \geqslant 1 \right\} \tag{5}$$

Let us consider now the interval $\mathcal{D}_\ell$. As $x^* \in \mathcal{D}_\ell$, it includes the *local unstable set* of x^* defined by

$$\mathbb{W}^u_{\ell oc}(x^*) = \left\{ x \in \mathcal{D}_\ell \mid \lim_{i\to\infty} f_\ell^{-i}(x) = x^* \right\} \tag{6}$$

By definition, the set $\mathbb{W}^u_{\ell oc}(x^*)$ consists of points to which the *local inverse* f_ℓ^{-1} applies. It can easily be shown that

$$\mathbb{W}^u(x^*) = \bigcup_{n\geqslant 0} f^n\left(\mathbb{W}^u_{\ell oc}(x^*)\right) \tag{7}$$

and that

$$\mathbb{W}^u_{\ell oc}(x^*) \subset \mathcal{D}_\ell \cap \mathcal{V}_\ell \tag{8}$$

In the most simple case, if f_ℓ is an increasing function on $\mathcal{D}_\ell$ and there are no stable fixed points of f in $\mathcal{D}_\ell$, then the local unstable set of x^* coincides with the interval $\mathcal{D}_\ell$, i.e. $\mathbb{W}^u_{\ell oc}(x^*) = \mathcal{D}_\ell$ (see Fig. 1(a)). If there are stable fixed points of f in $\mathcal{D}_\ell$, then the interval $\mathbb{W}^u_{\ell oc}(x^*)$ may be confined by two such fixed points (Fig. 1(b)) or by one such fixed point and one of the border points of $\mathcal{D}_\ell$ (Fig. 1(c)).

Similarly, if f_ℓ is a decreasing function on $\mathcal{D}_\ell$, then $\mathbb{W}^u_{\ell oc}(x^*)$ may coincide with $\mathcal{D}_\ell$ (Fig. 2(a)), may be confined by the points of a sTable 2-cycle (Fig. 2(b)) or by one border point of $\mathcal{D}_\ell$ and by its image by f_ℓ (Fig. 2(c)).

A point $q \in \mathbb{W}^u(x^*) \cap \mathbb{W}^s(x^*)$ is called homoclinic to x^*. By definition of $\mathbb{W}^u(x^*)$ and $\mathbb{W}^s(x^*)$, the sequence of images of q as well as a suitable sequence of preimages of q both converge to x^*. The union of these sequences gives an orbit homoclinic to x^* or, equivalently, a homoclinic orbit of x^*:

$$\begin{aligned} \mathcal{O}_{x^*}(q) = &\{x^* \leftarrow \ldots, q_{-i}, \ldots, q_{-1}, q, q_1, \ldots, q_m = x^*\} \\ &q_0 \equiv q,\ q_{i+1} = f(q_i) \text{ for } i = 0, \ldots, m-1 \\ &q_{-i-1} = f_{j_i}^{-1}(q_{-i}) \text{ for } i > 0,\ j_i \in \{1, \ldots, k\} \\ &q_m = x^*,\ \lim_{i\to\infty} q_{-i} = x^* \end{aligned} \tag{9}$$

Clearly, for each homoclinic orbit the point q can be chosen so that it belongs to $\mathbb{W}^u_{\ell oc}(x^*)$. Hence, the homoclinic orbit defined by Eq. (9) is equivalent to

$$\begin{aligned} \mathcal{O}_{x^*}(q) = &\{x^* \leftarrow \ldots, q_{-i}, \ldots, q_{-1}, q, q_1, \ldots, q_{m'} = x^*\} \\ &q_0 \equiv q,\ q_{i+1} = f(q_i) \text{ for } i = 0, \ldots, m'-1 \\ &q_{-i-1} = f_\ell^{-1}(q_{-i}) \text{ for } i > 0 \\ &q_{m'} = x^*,\ \lim_{i\to\infty} q_{-i} = x^* \end{aligned} \tag{10}$$

An example for a homoclinic orbit to the repelling fixed point $\mathcal{O}_\mathcal{R}$ of the logistic map

$$x_{n+1} = f(x_n) = \alpha x_n(1 - x_n) \tag{11}$$

is shown in Fig. 3(a). The intervals of monotonicity of the map are given by $\mathcal{D}_1 = \{x | x \leqslant \frac{1}{2}\}$ and $\mathcal{D}_2 = \{x | x \geqslant \frac{1}{2}\}$. The inverse functions on these intervals are

$$f_1^{-1}(x) = \frac{1}{2}\left(1 - \sqrt{1 - \frac{4x}{\alpha}}\right) \quad \text{and} \quad f_2^{-1}(x) = \frac{1}{2}\left(1 + \sqrt{1 - \frac{4x}{\alpha}}\right) \tag{12}$$

respectively. As one can see, the local unstable set $\mathbb{W}^u_{\ell oc}(\mathcal{O}_\mathcal{R}) \subset \mathcal{D}_2$ of the fixed point is bounded by the maximum point $x = \frac{1}{2}$ and its image by f. The only preimage of $\mathcal{O}_\mathcal{R}$ different from itself, namely the point $q = f_1^{-1}(\mathcal{O}_\mathcal{R})$ (see Fig. 3(a)) is located

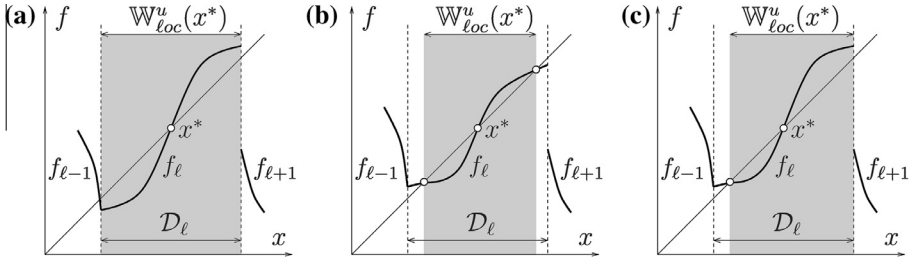

Fig. 1. Possible locations of the local unstable set $\mathbb{W}^u_{\ell oc}(x^*)$ of a repelling fixed point x^* in the case of an increasing branch f_ℓ.

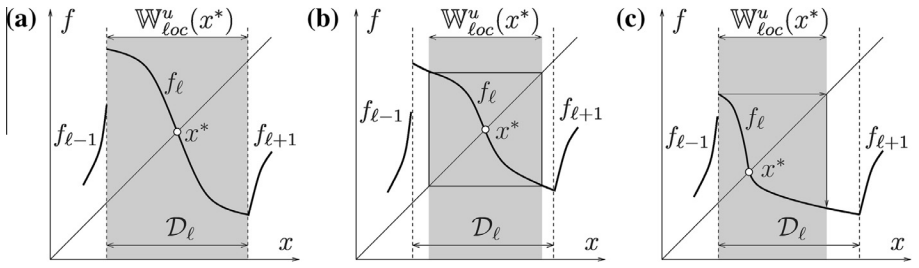

Fig. 2. Possible locations of the local unstable set $\mathbb{W}^u_{\ell oc}(x^*)$ of a repelling fixed point x^* in the case of a decreasing branch f_ℓ.

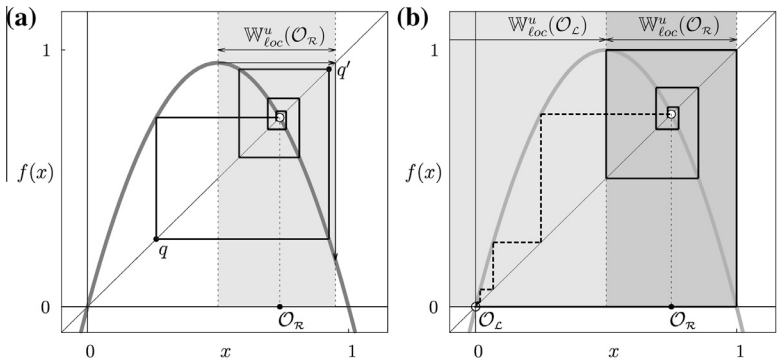

Fig. 3. (a) A homoclinic orbit to the repelling fixed point $\mathcal{O}_\mathcal{R}$ of the logistic map at $\alpha = 3.9$. The local unstable set $\mathbb{W}^u_{\ell oc}(\mathcal{O}_\mathcal{R})$ is marked. (b) The critical homoclinic connection between the repelling fixed point $\mathcal{O}_\mathcal{L}$ and $\mathcal{O}_\mathcal{R}$ of the logistic map at $\alpha = 4.0$. The local unstable sets $\mathbb{W}^u_{\ell oc}(\mathcal{O}_\mathcal{R})$ and $\mathbb{W}^u_{\ell oc}(\mathcal{O}_\mathcal{L})$ are marked.

outside $\mathbb{W}^u_{\ell oc}(\mathcal{O}_\mathcal{R})$, while the preimage of q by f_2^{-1} (the point q' in Fig. 3(a)) is located inside. Accordingly, when the homoclinic orbit shown in Fig. 3(a) is written using the point q', then it has the form given by Eq. (10) with $f_\ell^{-1} \equiv f_2^{-1}$.

A heteroclinic orbit between two repelling fixed points x^* and x^{**} is defined similarly. A point q belongs to a heteroclinic orbit from x^{**} to x^* if its forward orbit is mapped into x^* in a finite number of iterations, and a sequence of preimages of q tends to x^{**}. A heteroclinic orbit from x^{**} to x^* is a sequence of such points:

$$\begin{aligned} E^{x^*}_{x^{**}}(q) = &\{x^{**} \leftarrow \ldots, q_{-i}, \ldots, q_{-1}, q, q_1, \ldots, q_m = x^*\} \\ &q_0 \equiv q,\ q_{i+1} = f(q_i) \text{ for } i = 0, \ldots, m-1 \\ &q_{-i-1} = f_{j_i}^{-1}(q_{-i}) \text{ for } i > 0,\ j_i \in \{1, \ldots, k\} \\ &q_m = x^*,\ \lim_{i\to\infty} q_{-i} = x^{**} \end{aligned} \tag{13}$$

Following the same reasoning as above, for each heteroclinic orbit $E^{x^*}_{x^{**}}(q)$ the point q can be chosen so that it belongs to $\mathbb{W}^u_{\ell oc}(x^{**})$. Then the heteroclinic orbit defined by Eq. (13) is equivalent to

$$\begin{aligned} E^{x^*}_{x^{**}}(q) = &\{x^{**} \leftarrow \ldots, q_{-i}, \ldots, q_{-1}, q, q_1, \ldots, q_{m'} = x^*\} \\ &q_0 \equiv q,\ q_{i+1} = f(q_i) \text{ for } i = 0, \ldots, m'-1 \\ &q_{-i-1} = f_\ell^{-1}(q_{-i}) \text{ for } i > 0 \\ &q_{m'} = x^*,\ \lim_{i\to\infty} q_{-i} = x^{**} \end{aligned} \tag{14}$$

A heteroclinic connection $\mathcal{O}^{x^*}_{x^{**}}$ between two fixed points x^{**} and x^* is a union of two heteroclinic orbits, one from x^{**} to x^* and one from x^* to x^{**}:

$$\mathcal{O}^{x^*}_{x^{**}} = E^{x^*}_{x^{**}} \cup E^{x^{**}}_{x^*} \tag{15}$$

An example for a heteroclinic connection between two repelling fixed point of the logistic map is shown in Fig. 3(b).

A fixed point is called homoclinic iff there exists a homoclinic orbit to it; it is called one-side homoclinic iff all points homoclinic to it in the local unstable set $\mathbb{W}^u_{\ell oc}(x^*)$ are located on one side of it, and double-side homoclinic otherwise. Clearly, if a homoclinic fixed point belongs to a decreasing branch of f, it is necessarily double-side homoclinic. A homoclinic fixed point belonging to an increasing branch of f may be one-side or double-side homoclinic.

3. Basic idea of the algorithm

Depending on the particular task of investigation, several questions may be of interest. One may ask whether a specific fixed point or cycle is homoclinic or not. For a homoclinic fixed point or cycle the question may arise if it is one-side or double-side homoclinic. It may also be necessary to determine the sequence of applications of the inverse functions $f_j^{-1},\ j=1,\dots,k$, which leads from a given fixed point to its local unstable set.[1] Similar questions may also be asked for heteroclinic connections.

The basic idea behind the algorithm for solving the questions mentioned above follows immediately from the definition of homoclinic and heteroclinic orbits given by Eqs. (9) and (13), respectively. Accordingly, starting with a repelling fixed point x^* we can calculate the sequences of its preimages. If a sequence of preimages is found which converges to the point x^*, then this sequence belongs to a homoclinic orbit of x^* as given by Eq. (9). Similarly, if a sequence of preimages is found, which converges to a different repelling point x^{**}, then there exists a heteroclinic orbit from x^{**} to x^*, as given by Eq. (13). For simplicity, we only discuss the computation procedure for homoclinic orbits below, as the arguments for the calculation of heteroclinic orbits remain the same with the obvious exchange of one x^* by x^{**}.

From a practical point of view, this direct approach of computation of all the preimages is not feasible. Since each point p may have up to k preimages (namely $x_j = f_j^{-1}(p),\ j=1,\dots,k$, where k is the number of branches of monotonicity of f) the number of possible sequences of preimages up to rank m grows exponentially, as k^m. To improve the performance, the following two arguments can be used:

1. If a point x_j is located outside the invariant interval $\mathcal{I}$, its preimages do not need to be considered, as they can not enter the interval $\mathcal{I}$ again.
2. If a point x_j is located in the unstable set $\mathbb{W}^u(x^*)$, then the existence of a sequence of preimages of x_j which converges to x^* is guaranteed. Moreover, if x_j belongs to the local unstable set $\mathbb{W}^u_{\ell oc}(x^*)$, then this sequence is obtained by applying the corresponding local inverse.

Clearly, within the calculation procedure we can use instead of the complete unstable set $\mathbb{W}^u(x^*)$ any subset $\mathcal{T} \subset \mathbb{W}^u(x^*)$, denoted in the following as the *target set*. Obviously, the smaller the target set $\mathcal{T}$ is, the longer the sequence of preimages reaching $\mathcal{T}$ gets. Therefore, to increase the performance of the calculation procedure one has to take the target set as large as possible. However, the particular choice of the target set depends both on the investigation task and the properties of the investigated system.

- If the investigation task is to find a homoclinic orbit to x^* in the form given by Eq. (10)), then obviously the target set must be equal to the local unstable set x^*, i.e. $\mathcal{T} = \mathbb{W}^u_{\ell oc}(x^*)$.
- If the task is to determine whether the fixed point x^* is, for example, right-side homoclinic, then the left-side neighborhood of x^* must be excluded from consideration, i.e. $\mathcal{T} = \mathbb{W}^u_{\ell oc}(x^*) \cap \{x > x^*\}$.
- If the task is to decide whether x^* is homoclinic or not, and so the existence of a homoclinic orbit in the form given by Eq. (9)) is sufficient, then any $\mathcal{T} \subseteq \mathbb{W}^u(x^*)$ can be used.

The complete unstable set $\mathbb{W}^u(x^*)$ can be calculated by forward iteration of the set $\mathbb{W}^u_{\ell oc}(x^*)$, as given by Eq. (7). Recall that $\mathbb{W}^u_{\ell oc}(x^*)$ is an interval, while the stable set $\mathbb{W}^s(x^*)$ is in general a set of points. Therefore, when dealing with a particular system one has to decide which task is easier:

– calculation of the sequences of preimages belonging to the stable set $\mathbb{W}^s(x^*)$ (which requires a backward iteration of points),
– calculation of a larger interval $\mathcal{T} \subseteq \mathbb{W}^u(x^*)$ (which requires a forward iteration of intervals).

If the analytical expressions for the inverse functions $f_j^{-1}, j=1,\dots,k$, are explicitly known, as in the examples discussed below, the first choice is preferable. In this case we can use $\mathcal{T} = \mathbb{W}^u_{\ell oc}(x^*)$, so that $\mathcal{T}$ is a single interval, and obtain a homoclinic orbit in the form given in Eq. (10). In the opposite case, when the calculation of the preimages can be done only numerically and represents therefore a time-consuming step, the performance can be significantly improved using a larger set as a target set $\mathcal{T}$. In this case the target set $\mathcal{T}$ may be an interval or a finite collection of intervals, and a homoclinic orbit is obtained in the form given in Eq. (9).

The search procedure for heteroclinic orbits is similar with only one obvious difference regarding the target set. Namely, when searching for a heteroclinic orbit from x^{**} to x^*, then the target set $\mathcal{T}$ must be defined based on $W^u_{\ell oc}(x^{**})$, which belongs to the interval of monotonicity of f which contains the point x^{**}.

[1] As there are in general infinitely many sequences of preimages entering the local unstable set, corresponding to infinitely many homoclinic orbits, the question regards the shortest of them.

4. Implementation of the algorithm

As described in the previous section, the main task that has to be done in this approach is to determine the sequence of preimages, that leads from a given point x^* to a point in the target set $\mathcal{T}$. Since each point may have up to k preimages, this leads to a search algorithm in a k-nary tree.[2]

To guarantee that the search procedure terminates in the case that no connection from x^* to $\mathcal{T}$ exists, a suitable maximum preimage rank r_{max} has to be chosen. Therefore, during the search not only preimages located outside the invariant interval $\mathcal{I}$ but also preimages with rank higher than r_{max} are excluded from further consideration.

The search begins at the given repelling fixed point x^*. As x^* is a fixed point, its preimage by the local inverse is the point itself, so this preimage must be excluded from the search.

The search can terminate in three different ways. If a preimage is found that is inside the target set $\mathcal{T}$, the search is successful. If no such preimage is found, then two cases are possible. One is that there are no further preimages to continue the search, since all have been discarded because they were not located in the invariant interval $\mathcal{I}$. If this is the case then we can conclude that there cannot exist a connection from x^* to the target interval $\mathcal{T}$. The other possible case is that at least one preimage has been discarded because its rank was larger than the maximum preimage rank r_{max}. If that is the case, we can only conclude that no connection from x^* to the target interval $\mathcal{T}$ exists, that has a length smaller than or equal to r_{max}.

Following this reasoning, an algorithm to determine whether there exists a connection from a repelling fixed point x^* to the target set $\mathcal{T}$, can be outlined as shown in Listing 1.

Listing 1. Algorithm for the search for a connection from a repelling fixed point x^* to the target set $\mathcal{T}$.

```
1 Input: x*          the fixed point to check for a connection to T
         T           the target set
         I           the invariant interval
         r_max       the maximum preimage rank
         {f_j^-1, V_j}  the list of inverse functions and their domains,
                     j = 1,...,k
2 Output: "connection from x* to T found", or
          "connection from x* to T does not exist", or
          "connection from x* to T not found"
3 begin
4   S_p := [(x*, 0)]; i_max := 0;
5   while S_p is not empty do
6     (p, i) := the first element in S_p;
7     remove (p, i) from S_p;
8     if i ⩽ r_max then
9       i_max := max(i_max, i);
10        for each j ∈ 1,...,k do
11          if p ∈ V_j then
12            x := f_j^-1(p);
13            if x ∈ T & x ≠ x* then
14              return "connection from x* to T found";
15            if x ∈ I & x ≠ x* then
16              add (x, i + 1) to S_p;
17  if i_max = r_max then
18    return "connection from x* to T not found";
19  else
20    return "connection from x* to T does not exist";
```

The algorithm shown in that listing uses a data structure $\mathcal{S}_p$ in which elements of the form (p, k) are saved, with p being a preimage of x^* and k being the rank of that preimage. At each step of the calculation procedure the points saved in this data structure are leaf-nodes of the already processed sub-tree of the k-nary preimage tree.[3]

[2] A k-nary tree is a tree in which every node has at most k child nodes.

[3] Note that there is no need to save the interior nodes of the already processed sub-tree. Indeed, once processed, these nodes are no longer required for the search procedure. At the end of the search, if a point $q \in \mathcal{T}$ is found, these points could be used to output the chain of preimages leading from x^* to q (see the forward orbits of q in Eqs. (9)–(14)). However, as the point q is known, the same chain can easily be reproduced by forward iteration of q.

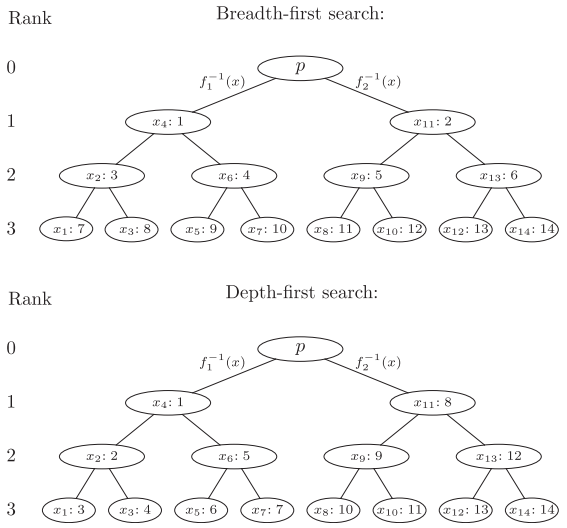

Fig. 4. Order in which the depth-first and breadth-first search procedures examine the rank-1, 2, 3 preimages $x_1, \ldots, x_{14}$ of a point p in a binary preimage tree.

One possible data structure which can be used for $\mathcal{S}_p$ is a queue. A queue (also called a first-in-first-out, FIFO, data structure) is a data structure that contains elements sorted according to the order in which they were saved in the queue. In a queue, new elements are added at the end (see line 16 in Listing 1), so that the first element of $\mathcal{S}_p$ is the oldest, and the last element is the newest one. Alternatively, instead of a queue a stack (also called a last-in-first-out, LIFO, data structure) can be used. In a stack, new elements are added at the beginning, so that the first element in $\mathcal{S}_p$ is the newest and the last element is the oldest one.

The difference between both approaches is that using a queue the algorithm performs a breadth-first search in the tree of preimages, and using a stack the algorithm performs a depth-first search. The basic idea of both approaches is illustrated in Fig. 4 which shows a binary tree of rank-k preimages, $k = 1, 2, 3$, of a point p, and the order in which these preimages are visited by the search procedure. Such a tree corresponds for example to the case in which all points of the invariant interval of a map have two preimages, as it is for the logistic map at $\alpha = 4$, see Fig. 3(b). In a breadth-first search the algorithm first investigates all preimages of rank i before it investigates the preimages of rank $i+1$, for all $i = 1, \ldots, r_{max} - 1$. Accordingly, the search procedure first visits the rank-1 preimages of p, for example first the left preimage x_4 and then the right preimage x_{11}. After that it continues with the rank-2 preimages, starting for example with the left preimage of x_4, i.e. the point x_2, then moving to the right preimage x_6, and so on. Note that the exact order in which the sibling nodes[4] are visited (or, in terms of the algorithm shown in Listing 1, the order in which the inverse functions f_j^{-1}, $j = 1, \ldots, k$ are applied to a particular point p) is not significant and specific to the implementation.

In a depth-first search for each preimage p the algorithm first investigates all preimages (of all ranks) that result from one inverse function $f_{i_1}^{-1}(p)$ before it investigates all preimages that result from another inverse function $f_{i_2}^{-1}(p), i_{1,2} \in \{1, \ldots, k\}$, and so on, until all preimages that can result from all inverse functions have been considered. In the example shown in Fig. 4 this means that first the points x_4, x_2 and x_1 are visited, as they result from the application of the function f_1^{-1}.

Both kinds of search procedures will lead to the same output, however they differ in memory requirements (meaning the maximum number of preimages that are saved in $\mathcal{S}_p$ at the same time during the search) and search performance. In the worst case (meaning that during the search no preimages outside the invariant interval appear, and that no connection to the target set is found), the memory requirements of breadth-first search are much higher than for depth-first search. During a breadth-first search, all preimages of rank n have to be saved in $\mathcal{S}_p$ before they can be processed. In the worst case, this means that all preimages of rank r_{max} have to be saved in $\mathcal{S}_p$, which are $k^{r_{max}}$ preimages.

For the worst case of a depth-first search, the situation is different. In the k-nary preimage tree, each node has at most k child nodes. At any time during a depth-first search, for each rank of the tree, only the child nodes of one node of that rank need to be saved in $\mathcal{S}_p$. During the search, one preimage of rank n must be removed before the preimages of rank $n+1$ are saved in $\mathcal{S}_p$, until the maximum rank r_{max} is reached. This means that for each rank smaller than r_{max} at most $(k-1)$ preimages are saved in $\mathcal{S}_p$, and for rank r_{max} at most k preimages are saved in

[4] Nodes with a common parent-node.

$\mathcal{S}_p$. Therefore the number of nodes saved in $\mathcal{S}_p$ in the worst case of a depth-fist search is $(r_{max}-1)(k-1)+k$. A detailed analysis of the memory requirements in the average case is beyond the scope of this work, though it can be argued that in most cases depth-first search requires less memory than breadth-first search, using similar arguments as for the worst case.

Regarding the search performance, both search procedures perform equally well in the worst case. Again, a detailed analysis of the average case is beyond the scope of this work.

Finally, note that breadth-first has a specific advantage over depth-first search. If the k-nary preimage tree contains multiple preimages in the target set, then breadth-first search is guaranteed to find the preimage with the smallest rank. In contrast to that, depth-first search is only guaranteed to find one of these preimages, of arbitrary rank.

The question may arise how the presented algorithm works when implemented on a computer, using a finite representation of numbers and how stable it is with respect to rounding errors and other inaccuracies. In particular, when the inverse functions are calculated numerically, the computed values of the preimages are not precise. However, the algorithm is robust with respect to these inaccuracies. What is significant for the algorithm is the fact that some preimage belongs to the target interval, but not the exact value of this preimage. The only case in which the algorithm may fail due to the numerical inaccuracy is when a preimage is located closer to the boundary of some domain $\mathcal{V}_j$ than the deviation caused by this inaccuracy. In other words, what may be affected by these problems is the calculation of very long paths to the target interval for parameter values which are very close to homoclinic bifurcation points.

5. Remarks on cycles

The algorithm described above is designed for finding homoclinic orbits and heteroclinic connections of fixed points. In principle, by using the appropriate iterate, it can also be applied to cycles. Indeed, the investigation of the properties of an n-cycle can be reduced to the investigation of any one of n associated fixed points of the iterate f^n. The intervals of monotonicity of f^n are bounded by points which confine the intervals of monotonicity of the original function f, and by their preimages. Similarly, when dealing with a heteroclinic connection from an n-cycle to an m-cycle, we can investigate heteroclinic connections between corresponding fixed points of the iterate f^N where $N=\mathrm{lcm}(n,m)$ is the least common multiple of the numbers $n$and m. However, in practice this can lead to problems.

To do its work, the algorithm needs inverse functions and their domains for each interval of monotonicity of the iterate. Recall that the number of these intervals grows exponentially with the order of the iterate. So, for example when dealing with a function f which has only two intervals of monotonicity, and when searching for a heteroclinic connection between a 3-cycle and a 4-cycle, one has to deal with the iterate f^{12}, which may have up to $2^{12}=4096$ intervals of monotonicity. In this case it is possible to provide the inverse functions analytically only if the function f is piecewise linear. Otherwise on each of the relevant partitions the equation $f^{12}(y)=x$ must be solved numerically, which may be require a significant calculational effort. Moreover, suppose for example that on both intervals of monotonicity the function f is quadratic. Then it is easy to see that the calculation of the inverse may be a highly ill-conditioned problem. Therefore, the question arises if an alternative way is possible.

In fact, instead of the iterate, the original function f can be used. This makes the application of the algorithm considerably easier, as illustrated below. However, if the algorithm is used this way, some minor modifications are necessary, due to details discussed below.

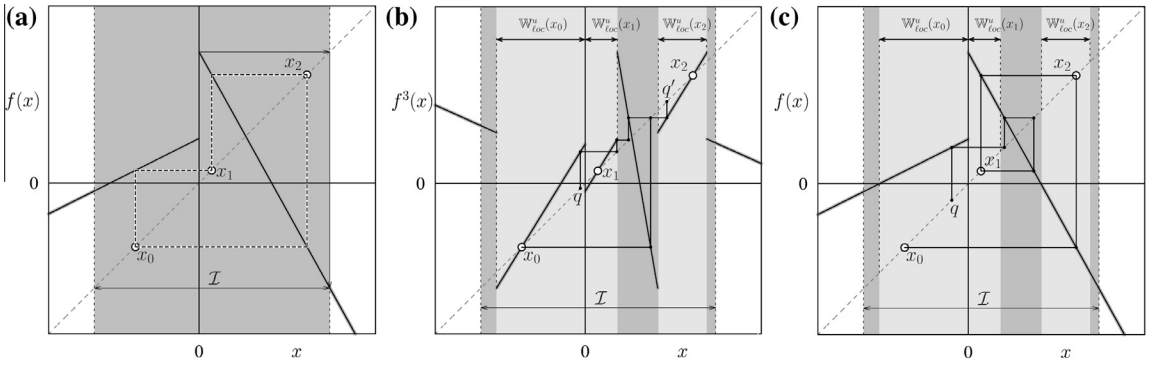

Fig. 5. (a) Repelling cycle $\mathcal{O}_{\mathcal{LR}^2}$ of map (1). (b) Shortest chains of preimages by the inverses of f^3 of the point x_0 leading to the local unstable set $\mathbb{W}^u_{loc}(x_0)$ of the point x_0 (the point q) or to the local unstable set $\mathbb{W}^u_{loc}(\mathcal{O}_{\mathcal{LR}^2})$ of the cycle (the point q'). (c) Shortest chain of preimages by the inverses of f of the point x_0 leading to $\mathbb{W}^u_{loc}(x_0)$ and $\mathbb{W}^u_{loc}(\mathcal{O}_{\mathcal{LR}^2})$ (the point q). Parameters: $a_\ell=0.5,\ a_r=-1.8,\ \mu_\ell=0.34,\ \mu_r=1$.

If the algorithm is used to search for a homoclinic connection of a point x^* of an n-cycle $\mathcal{O} = \{x_0, \ldots, x_{n-1}\}$, then the target set can be defined in a similar way as described in Section 2 for fixed points. For each of the points x_i, $i = 0, \ldots, n-1$ the local unstable set $\mathbb{W}^u_{\ell oc}(x_i)$ is defined by Eq. (6) using the local inverse of the nth iterate f^n. However, when starting with some point of the cycle, for example x_0, one can use as target set not only the local unstable set of this point, i.e. $\mathcal{T} = \mathbb{W}^u_{\ell oc}(x_0)$, but also the local unstable set of the cycle, which is defined by

$$\mathbb{W}^u_{\ell oc}(\mathcal{O}) = \bigcup_{i=0}^{n-1} \mathbb{W}^u_{\ell oc}(x_i) \tag{16}$$

Indeed, if a preimage of x_0 is found in a set $\mathbb{W}^u_{\ell oc}(x_i)$ with $i \neq 0$, then its preimage by f belongs to $\mathbb{W}^u_{\ell oc}(x_{i-1})$. Applied iteratively at most $n-1$ times, this proves the existence of a preimage of x_0 which belongs to $\mathbb{W}^u_{\ell oc}(x_i)$.

Recall that when dealing with a fixed point x^*, its preimage by the local inverse is excluded from consideration, as it is the fixed point itself. If for example the target set is chosen as $\mathcal{T} = \mathbb{W}^u_{\ell oc}(x^*)$, then obviously $x^* \in \mathcal{T}$, but this fact has no relevance for the existence or non-existence of an orbit homoclinic to x^*. In the algorithm shown in Listing 1 this is done by the condition

$$x \neq x^* \tag{17}$$

in lines 13 and 15. When dealing with a cycle, it seems to be natural to replace this condition by

$$x \notin \{x_0, \ldots, x_{n-1}\} \tag{18}$$

Independent of the definition of the target set, in all three possible cases $\mathcal{T} = \mathbb{W}^u_{\ell oc}(\mathcal{O})$, $\mathcal{T} \subset \mathbb{W}^u_{\ell oc}(\mathcal{O})$, and $\mathbb{W}^u_{\ell oc}(\mathcal{O}) \subset \mathcal{T} \subset \mathbb{W}^u(\mathcal{O})$, the fact that the points of the cycle belong to the target set does not have any meaning for the existence of a connection from the cycle to the target set. However, if the condition (17) is replaced by the condition (18), the results may be wrong.

To explain the possible problem let us consider as an example the piecewise linear map

$$x_{n+1} = f(x_n) = \begin{cases} f_\ell(x_n) = a_\ell x_n + \mu_\ell & \text{if } x_n < 0 \\ f_r(x_n) = a_r x_n + \mu_r & \text{if } x_n > 0 \end{cases} \tag{19}$$

In the configuration illustrated in Fig. 5, the map has a globally attracting invariant absorbing interval

$$\mathcal{I} = \left(f_r^2(0), f_r(0)\right) \tag{20}$$

which contains, among other invariant sets, the repelling 3-cycle $\mathcal{O}_{\mathcal{LR}^2}$ (see Fig. 5(a)). The question we are interested in is whether this cycle is homoclinic at the considered parameter values. Applying the algorithm for fixed points we may consider any one of the points of the cycle, which are fixed points of the third iterate, for example the first one, marked with x_0 in Fig. 5. As the target set we can choose the local unstable set of this point, which is given by

$$\mathcal{T} = \mathbb{W}^u_{\ell oc}(x_0) = \left(f_\ell^{-1}(0), 0\right) \tag{21}$$

Then the algorithm can easily find a chain of preimages of x_0 which reaches the point $q \in \mathcal{T}$ in four steps, as shown in Fig. 5(b). Moreover, when the local unstable set of the complete cycle is used as the target set, i.e.

$$\mathcal{T} = \mathbb{W}^u_{\ell oc}\left(\mathcal{O}_{\mathcal{LR}^2}\right) = \mathbb{W}^u_{\ell oc}(x_0) \cup \mathbb{W}^u_{\ell oc}(x_1) \cup \mathbb{W}^u_{\ell oc}(x_2) \tag{22}$$

where

$$\mathbb{W}^u_{\ell oc}(x_0) = \left(f_\ell^{-1}(0), 0\right) \tag{23a}$$
$$\mathbb{W}^u_{\ell oc}(x_1) = \left(0, f_r^{-1} \circ f_r^{-1}(0)\right) \tag{23b}$$
$$\mathbb{W}^u_{\ell oc}(x_2) = \left(f_r^{-1}(0), f_r^{-1} \circ f_\ell^{-1}(0)\right) \tag{23c}$$

then the algorithm terminates faster, finding a chain of preimages of x_0 which reaches the point $q' \in \mathcal{T}$ in two steps (see in Fig. 5(b)). However, to obtain this result we need to provide the algorithm with the list of inverses for the relevant branches of f^3 (clearly, a branch f_j^3 is relevant iff $\mathcal{D}_j \cap \mathcal{I} \neq \emptyset$). At the considered parameter values the iterate f^3 is given by

$$f^3(x) = \begin{cases} f_{\ell\ell\ell}(x) = f_\ell \circ f_\ell \circ f_\ell(x) & \text{if } x \in \mathcal{D}_{\ell\ell\ell} = \left(-\infty, f_\ell^{-1} \circ f_\ell^{-1}(0)\right) \\ f_{\ell\ell r}(x) = f_r \circ f_\ell \circ f_\ell(x) & \text{if } x \in \mathcal{D}_{\ell\ell r} = \left(f_\ell^{-1} \circ f_\ell^{-1}(0), f_\ell^{-1}(0)\right) \\ f_{\ell r r}(x) = f_r \circ f_r \circ f_\ell(x) & \text{if } x \in \mathcal{D}_{\ell r r} = \left(f_\ell^{-1}(0), 0\right) \\ f_{r r \ell}(x) = f_\ell \circ f_r \circ f_r(x) & \text{if } x \in \mathcal{D}_{r r \ell} = \left(0, f_r^{-1} \circ f_r^{-1}(0)\right) \\ f_{r r r}(x) = f_r \circ f_r \circ f_r(x) & \text{if } x \in \mathcal{D}_{r r r} = \left(f_r^{-1} \circ f_r^{-1}(0), f_r^{-1}(0)\right) \\ f_{r\ell r}(x) = f_r \circ f_\ell \circ f_r(x) & \text{if } x \in \mathcal{D}_{r\ell r} = \left(f_r^{-1}(0), f_r^{-1} \circ f_\ell^{-1}(0)\right) \\ f_{r\ell\ell}(x) = f_\ell \circ f_\ell \circ f_r(x) & \text{if } x \in \mathcal{D}_{r\ell\ell} = \left(f_r^{-1} \circ f_\ell^{-1}(0), \infty\right) \end{cases} \tag{24}$$

As one can see in Fig. 5(b), six of seven branches of f^3 have a non-empty intersection with $\mathcal{I}$, so that the required list of inverses with their domains is given by

$$\begin{aligned}
&\{[f^{-1}_{\ell\ell r} = f_r^{-1} \circ f_\ell^{-1} \circ f_\ell^{-1}, \mathcal{V}_{\ell\ell r} = f_{\ell\ell r}(\mathcal{D}_{\ell\ell r}) = (f_r \circ f_\ell(0), f_r(0))],\\
&[f^{-1}_{\ell r r} = f_r^{-1} \circ f_r^{-1} \circ f_\ell^{-1}, \mathcal{V}_{\ell r r} = f_{\ell r r}(\mathcal{D}_{\ell r r}) = (f_r \circ f_r(0), f_r \circ f_r \circ f_\ell(0))],\\
&[f^{-1}_{r r \ell} = f_\ell^{-1} \circ f_r^{-1} \circ f_r^{-1}, \mathcal{V}_{r r \ell} = f_{r r \ell}(\mathcal{D}_{r r \ell}) = (f_\ell \circ f_r \circ f_r(0), f_\ell(0))],\\
&[f^{-1}_{r r r} = f_r^{-1} \circ f_r^{-1} \circ f_r^{-1}, \mathcal{V}_{r r r} = f_{r r r}(\mathcal{D}_{r r r}) = (f_r \circ f_r(0), f_r(0))],\\
&[f^{-1}_{r \ell r} = f_r^{-1} \circ f_\ell^{-1} \circ f_r^{-1}, \mathcal{V}_{r \ell r} = f_{r \ell r}(\mathcal{D}_{r \ell r}) = (f_r \circ f_\ell(0), f_r(0))],\\
&[f^{-1}_{r \ell \ell} = f_\ell^{-1} \circ f_\ell^{-1} \circ f_r^{-1}, \mathcal{V}_{r \ell \ell} = f_{r \ell \ell}(\mathcal{D}_{r \ell \ell}) = (-\infty, f_\ell(0))]\}
\end{aligned} \tag{25}$$

where the inverse functions f_ℓ^{-1} and f_r^{-1} are given by

$$f_\ell^{-1}(x) = \frac{1}{a_\ell}(x - \mu_\ell) \quad \text{and} \quad f_r^{-1}(x) = \frac{1}{a_r}(x - \mu_r) \tag{26}$$

In general, it may become a quite extensive and time-consuming task to provide the algorithm with a list similar to the one given by Eq. (25). In particular, if the algorithm is applied under variation of parameters, then some branches of the iterate may become irrelevant (leave the invariant interval or disappear completely), while new branches may appear. Clearly, it is much easier to work with the branches of f, in which case instead of the list given by Eq. (25) we have just

$$\{[f_\ell^{-1}, \mathcal{V}_\ell = (-\infty, \mu_\ell)], [f_r^{-1}, \mathcal{V}_r = (-\infty, \mu_r)]\} \tag{27}$$

However, if condition (17) is replaced by condition (18) in both the lines 13 and 15 in Listing 1, and the list given by Eq. (27) is used instead of the one given by Eq. (25), then we obtain a wrong result when starting from the point $x_0^{\mathcal{LR}^2}$. Indeed, the preimage of this point by f_r^{-1} belongs to the cycle (the point $x_2^{\mathcal{LR}^2}$) and the preimage by f_ℓ^{-1} is located outside the interval $\mathcal{I}$. So, in this way no chain of preimages of $x_0^{\mathcal{LR}^2}$ leading to the target set can be found.

Listing 2. Modifications of the algorithm shown in Listing 1. The resulting algorithm searches for a connection from a repelling cycle to the target set $\mathcal{T}$.

```
   Input: {x_0, ..., x_{n-1}}    the cycle to check for a connection to T
   ..........................
   begin
     ..........................
 4   x* := x_0; S_p := [(x*, 0)]; i_max := 0;
     ..........................
13   if x ∈ T & x ∉ {x_0, ..., x_{n-1}} then
14     return "connection from x* to T found";
15   if x ∈ I & x ≠ x* then
16   add (x, i + 1) to S_p;
     ..........................
```

In principle, to solve the described problem, one can apply the algorithm to all the points of the cycle and then conclude that there is a chain of preimages leading from the cycle to the target set if it is found for at least one of the points. However, the problem can be solved much easier by modifying the line 13 and *not* modifying the line 15, as shown in Listing 2. The condition in line 15 implies that the points of the cycle are added to the list of preimages of x_0. The condition (17) in line 15 guarantees now that the process is stopped at the point x_{n-1} (supposing that $n < r_{max}$) and can not become cyclic. Although the points of the cycle may belong to $\mathcal{T}$, this does not influence the result of the algorithm, due to the condition in line 13. However, the preimages of all these points are now taken into consideration, and this solves the problem described above. For example, as one can see in Fig. 5(c), the chain of preimages leading from x_0 to $\mathcal{T}$ (independent of whether the definition of $\mathcal{T}$ is given by Eq. (21) or by Eq. (22)) includes the points x_2 and x_1 (which is the only preimage of x_2). The point x_1 has two preimages, of which the left one is excluded from consideration, by the line 15 of the algorithm, as it is the starting point x_0. The right preimage of x_1 leads to the point $q \in \mathcal{T}$, which proves that the cycle is homoclinic.

6. Application examples

As already mentioned, the algorithm described above can be of help not only to clarify whether a fixed point or a cycle is homoclinic or not, but also for the description of homoclinic bifurcations and their sequences.

Let us now illustrate this using the map (19) and the example shown in Fig. 6. Note that since $\mu_\ell \neq \mu_r$ the map is discontinuous at the considered parameter combination. The sequence of bifurcations shown in Fig. 6 leads from a one-band cha-

otic attractor to a six-band chaotic attractor, then to a three-band one, and eventually back to a one-band chaotic attractor. It is well-known that particular bifurcations in this sequence are related to homoclinic bifurcations of repelling cycles. In particular, the bifurcation leading from a one-band to a six-band chaotic attractor (marked in Fig. 6 with $\eta^1_{\mathcal{LR}^2}$) can immediately be recognized as an expansion bifurcation (interior crisis), related to a homoclinic bifurcation of a repelling three-cycle $\mathcal{O}_{\mathcal{LR}^2}$. As mentioned in [2], an expansion bifurcation is related to a homoclinic bifurcation of a cycle with a positive eigenvalue, which is necessarily homoclinic on one side of the bifurcation point, while on the other side it may be one-side homoclinic or non-homoclinic.

Regarding the cycle $\mathcal{O}_{\mathcal{LR}^2}$ one can see immediately that its eigenvalue is $\lambda = a_\ell a_r^2 > 0$ (as $a_\ell > 0$). This cycle begins to exist at the border collision bifurcation $\xi_{\mathcal{LR}^2}$, which takes place inside the chaotic attractor, so one can assume that the cycle is already homoclinic when it appears. The points of the cycle are given by

$$\begin{aligned} x_0^{\mathcal{LR}^2} &= -\frac{a_\ell a_r \mu_r + a_r \mu_\ell + \mu_r}{a_\ell a_r^2 - 1} \\ x_1^{\mathcal{LR}^2} &= -\frac{a_r^2 \mu_\ell + a_r \mu_r + \mu_r}{a_\ell a_r^2 - 1} \\ x_2^{\mathcal{LR}^2} &= -\frac{a_\ell a_r \mu_r + a_\ell \mu_r + \mu_\ell}{a_\ell a_r^2 - 1} \end{aligned} \tag{28}$$

with $x_0^{\mathcal{LR}^2} < 0 < x_1^{\mathcal{LR}^2} < x_2^{\mathcal{LR}^2}$. In the considered parameter ranges the local unstable set $\mathbb{W}^u_{\ell oc}(\mathcal{O}_{\mathcal{LR}^2})$ is given by

$$\mathbb{W}^u_{\ell oc}(\mathcal{O}_{\mathcal{LR}^2}) = \mathbb{W}^u_{\ell oc}\left(x_0^{\mathcal{LR}^2}\right) \cup \mathbb{W}^u_{\ell oc}\left(x_1^{\mathcal{LR}^2}\right) \cup \mathbb{W}^u_{\ell oc}\left(x_2^{\mathcal{LR}^2}\right) \tag{29a}$$

with

$$\mathbb{W}^u_{\ell oc}\left(x_0^{\mathcal{LR}^2}\right) = \left(f_\ell^{-1}(0), f_\ell^{-1} \circ f_r^{-1}(0)\right) \tag{29b}$$

$$\mathbb{W}^u_{\ell oc}\left(x_1^{\mathcal{LR}^2}\right) = \left(0, f_r^{-1} \circ f_r^{-1}(0)\right) \tag{29c}$$

$$\mathbb{W}^u_{\ell oc}\left(x_2^{\mathcal{LR}^2}\right) = \left(f_r^{-1}(0), f_r^{-1} \circ f_\ell^{-1}(0)\right) \tag{29d}$$

At the moment of the expansion bifurcation the points of the cycle collide with images of the critical point $c_\ell = f_\ell(0)$, which determine the boundaries of the six-band chaotic attractor after the bifurcation, so that the condition of the bifurcation is given by any one of the equations

$$x_0^{\mathcal{LR}^2} = f^4 \circ f_\ell(0), \quad x_1^{\mathcal{LR}^2} = f^5 \circ f_\ell(0), \quad \text{or} \quad x_2^{\mathcal{LR}^2} = f^3 \circ f_\ell(0) \tag{30}$$

Still, the question remains whether the cycle $\mathcal{O}_{\mathcal{LR}^2}$ is one-side homoclinic or non-homoclinic after the expansion bifurcation.

Applying the algorithm, we confirm that before the expansion bifurcation $\eta^1_{\mathcal{LR}^2}$ the cycle $\mathcal{O}_{\mathcal{LR}^2}$ is homoclinic from both sides and we show that after the bifurcation it is one-side homoclinic. In order to check that the cycle is homoclinic from one side, we use the target set

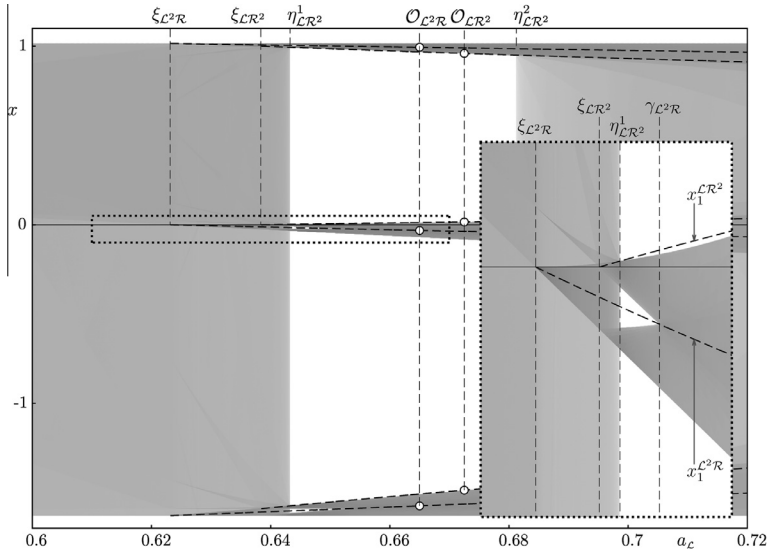

Fig. 6. Transition from a one-band to a 6-band chaotic attractor in map (19). Parameters: $a_r = -2.59$, $\mu_\ell = 1.015$, $\mu_r = 1$.

$$\mathcal{T}_\ell = \left(f_\ell^{-1}(0), x_0^{\mathcal{LR}^2}\right) \cup \left(0, x_1^{\mathcal{LR}^2}\right) \cup \left(x_2^{\mathcal{LR}^2}, f_r^{-1} \circ f_\ell^{-1}(0)\right) \tag{31}$$

and to check that it is homoclinic from the other side, the target set

$$\mathcal{T}_r = \left(x_0^{\mathcal{LR}^2}, f_\ell^{-1} \circ f_r^{-1}(0)\right) \cup \left(x_1^{\mathcal{LR}^2}, f_r^{-1} \circ f_r^{-1}(0)\right) \cup \left(f_r^{-1}(0), x_2^{\mathcal{LR}^2}\right) \tag{32}$$

Clearly, the sets $\mathcal{T}_\ell$ and $\mathcal{T}_r$ are defined as subsets of $\mathbb{W}^u_{\ell oc}(\mathcal{O}_{\mathcal{LR}^2})$ located on one side of the cycle (see Eqs. (28) and (29)). As explained above, we use for the calculations the function f and not f^3, so that the required list of inverses is given by Eq. (27) (see also Eq. (26)). To obtain all the results the value $r_{max} = 12$ was used.

For the parameter value $a_\ell = 0.64$, which is located between the value $a_\ell \approx 0.63835$ of the border collision bifurcation $\xi_{\mathcal{LR}^2}$ and the value $a_\ell \approx 0.643258$ of the expansion bifurcation $\eta^1_{\mathcal{LR}^2}$, we obtain from Eqs. (31) and (32)

$$\mathcal{T}_\ell \approx (-1.58594, -1.58470) \cup \left(0, 7.89509 \cdot 10^{-4}\right) \cup (0.99796, 0.99843)$$
$$\mathcal{T}_r \approx (-1.58470, -0.98265) \cup \left(7.89509 \cdot 10^{-4}, 0.23703\right) \cup (0.38610, 0.99796)$$

and the algorithm detects the points

$$q = f_r^{-1} \circ f_r^{-1} \circ f_\ell^{-1} \circ f_\ell^{-1} \circ f_r^{-1} \circ f_\ell^{-1} \circ f_\ell^{-1} \circ f_r^{-1}\left(x_0^{\mathcal{LR}^2}\right) \approx 4.23054 \cdot 10^{-4} \in \mathcal{T}_\ell$$
$$q' = f_r^{-1} \circ f_\ell^{-1} \circ f_r^{-1}\left(x_0^{\mathcal{LR}^2}\right) \approx 0.39638 \in \mathcal{T}_r$$

which confirm that the cycle is double-side homoclinic before the expansion bifurcation as expected. Similarly, after the bifurcation, at the parameter value $a_\ell = 0.67$, the target sets are given by

$$\mathcal{T}_\ell \approx (-1.51492, -1.49344) \cup (0, 0.14394) \cup (0.96271, 0.97101)$$
$$\mathcal{T}_r \approx (-1.49344, -0.93866) \cup (0.14394, 0.23703) \cup (0.38610, 0.96271)$$

and the algorithm detects the point

$$q' = f_r^{-1} \circ f_\ell^{-1} \circ f_r^{-1}\left(x_0^{\mathcal{LR}^2}\right) \approx 0.41623 \in \mathcal{T}_r$$

but no points in the target set $\mathcal{T}_\ell$ can be detected. Accordingly, we conclude that the cycle after the bifurcation is one-side homoclinic.

Regarding the other 3-cycle shown in Fig. 6, namely the cycle $\mathcal{O}_{\mathcal{L}^2\mathcal{R}}$, the situation is significantly more sophisticated. On the one hand, similar to the cycle $\mathcal{O}_{\mathcal{LR}^2}$, it appears at a border collision bifurcation (marked with $\xi_{\mathcal{L}^2\mathcal{R}}$ in Fig. 6) being already homoclinic. On the other hand, at the parameter value marked with $\gamma_{\mathcal{L}^2\mathcal{R}}$ in Fig. 6 it undergoes a homoclinic bifurcation related to a pairwise merging of the bands of the chaotic attractor (a transition from a six-band to a three-band chaotic attractor). As mentioned in [2], such a merging bifurcation is related to a homoclinic bifurcation of a cycle with a negative eigenvalue, which is necessarily non-homoclinic before the bifurcation and homoclinic after. Indeed, the eigenvalue $\lambda = a_\ell^2 a_r < 0$ of the cycle $\mathcal{O}_{\mathcal{L}^2\mathcal{R}}$ is negative (as $a_r < 0$). However, if the cycle $\mathcal{O}_{\mathcal{L}^2\mathcal{R}}$ is homoclinic immediately after the border collision bifurcation $\xi_{\mathcal{L}^2\mathcal{R}}$, but not homoclinic between the expansion bifurcation $\eta^1_{\mathcal{LR}^2}$ and the merging bifurcation $\gamma_{\mathcal{L}^2\mathcal{R}}$, then the question arises at which point it becomes non-homoclinic. The most obvious assumption is that it happens at the point $\eta^1_{\mathcal{LR}^2}$. However, if the cycle $\mathcal{O}_{\mathcal{L}^2\mathcal{R}}$ undergoes a homoclinic bifurcation at $\eta^1_{\mathcal{LR}^2}$, it must be associated with the presence of a critical homoclinic orbit, that means a critical point must be preperiodic to the cycle $\mathcal{O}_{\mathcal{L}^2\mathcal{R}}$. This can not be the point $c_\ell = f_\ell(0)$, since at $\eta^1_{\mathcal{LR}^2}$ it is preperiodic to the cycle $\mathcal{O}_{\mathcal{LR}^2}$. Moreover, it can be shown that this can also not be the point $c_r = f_r(0)$, as otherwise the bifurcation occurring at the parameter point $\eta^1_{\mathcal{LR}^2}$ would be a codimension-two bifurcation. As the map has only two critical points, the situation seems to be contradictory and requires further consideration.

For the cycle $\mathcal{O}_{\mathcal{L}^2\mathcal{R}}$ we obtain immediately that its points are given by

$$\begin{aligned} x_0^{\mathcal{L}^2\mathcal{R}} &= -\frac{a_\ell^2 \mu_r + a_\ell \mu_\ell + \mu_\ell}{a_\ell^2 a_r - 1} \\ x_1^{\mathcal{L}^2\mathcal{R}} &= -\frac{a_\ell^2 \mu_r + a_\ell \mu_\ell + \mu_\ell}{a_\ell^2 a_r - 1} \\ x_2^{\mathcal{L}^2\mathcal{R}} &= -\frac{a_r a_\ell \mu_\ell + a_\ell \mu_r + \mu_\ell}{a_\ell^2 a_r - 1} \end{aligned} \tag{33}$$

with $x_0^{\mathcal{L}^2\mathcal{R}} < x_1^{\mathcal{L}^2\mathcal{R}} < 0 < x_2^{\mathcal{L}^2\mathcal{R}}$. and that its local unstable set in the considered parameter ranges is given by

$$\mathbb{W}^u_{\ell oc}(\mathcal{O}_{\mathcal{L}^2\mathcal{R}}) = \mathbb{W}^u_{\ell oc}\left(x_0^{\mathcal{L}^2\mathcal{R}}\right) \cup \mathbb{W}^u_{\ell oc}\left(x_1^{\mathcal{L}^2\mathcal{R}}\right) \cup \mathbb{W}^u_{\ell oc}\left(x_2^{\mathcal{L}^2\mathcal{R}}\right) \tag{34a}$$

with

$$\mathbb{W}^u_{\ell oc}\left(x_0^{\mathcal{L}^2\mathcal{R}}\right) = \left(f_\ell^{-1} \circ f_\ell^{-1} \circ f_r^{-1} \circ f_\ell^{-1}(0), f_\ell^{-1}(0)\right) \tag{34b}$$

$$\mathbb{W}^u_{\ell oc}\left(x_1^{\mathcal{L}^2\mathcal{R}}\right) = \left(f_\ell^{-1} \circ f_r^{-1} \circ f_\ell^{-1}(0), 0\right) \tag{34c}$$

$$\mathbb{W}^u_{\ell oc}\left(x_2^{\mathcal{L}^2\mathcal{R}}\right) = \left(f_r^{-1} \circ f_\ell^{-1}(0), f_r^{-1} \circ f_\ell^{-1} \circ f_\ell^{-1} \circ f_r^{-1} \circ f_\ell^{-1}(0)\right) \tag{34d}$$

In the following we use the target set $\mathcal{T} = \mathbb{W}^u_{\ell oc}(\mathcal{O}_{\mathcal{L}^2\mathcal{R}})$. Applying the algorithm, we confirm that the cycle $\mathcal{O}_{\mathcal{L}^2\mathcal{R}}$ is indeed homoclinic immediately after it appearance via the border collision bifurcation $\xi_{\mathcal{L}^2\mathcal{R}}$ at $a_\ell \approx 0.62314$. At $a_\ell = 0.63$ the target set is given by

$$\mathcal{T} \approx (-1.62837, -1.61111) \cup (-0.01087, 0) \cup (1.00815, 1.01481)$$

and the algorithm detects the point

$$\begin{aligned} q = {} & f_\ell^{-1} \circ f_r^{-1} \circ f_\ell^{-1} \circ f_\ell^{-1} \circ f_r^{-1} \circ f_\ell^{-1} \circ f_r^{-1} \circ f_r^{-1} \circ f_\ell^{-1} \circ f_r^{-1} \circ f_r^{-1} \circ f_\ell^{-1} \circ f_r^{-1} \circ \\ & f_r^{-1} \circ f_\ell^{-1} \circ f_r^{-1} \circ f_r^{-1} \circ f_r^{-1} \circ f_\ell^{-1} \circ f_r^{-1} \circ f_\ell^{-1} \circ f_r^{-1} \circ f_\ell^{-1} \circ f_r^{-1}\left(x_0^{\mathcal{L}^2\mathcal{R}}\right) \\ \approx {} & -1.71651 \cdot 10^{-4} \in \mathcal{T} \end{aligned}$$

belonging to this set. As expected, the cycle is also homoclinic after the merging bifurcation $\gamma_{\mathcal{L}^2\mathcal{R}}$. At $a_\ell = 0.67$ the target set is given by

$$\mathcal{T} \approx (-1.61291, -1.51493) \cup (-0.06565, 0) \cup (0.97101, 1.00885)$$

and the algorithm detects the point

$$q = f_\ell^{-1} \circ f_r^{-1} \circ f_\ell^{-1} \circ f_\ell^{-1} \circ f_r^{-1} \circ f_\ell^{-1} \circ f_r^{-1} \circ f_r^{-1}\left(x_0^{\mathcal{L}^2\mathcal{R}}\right) \approx 6.71449 \cdot 10^{-3} \in \mathcal{T}$$

belonging to this set. However, for the values of a_ℓ between $\xi_{\mathcal{L}\mathcal{R}^2}$ and $\eta^1_{\mathcal{L}\mathcal{R}^2}$ the algorithm does not find a connection from the cycle to the used target interval.

The situation described above is explained as follows. As a_ℓ approaches the value corresponding to the border collision bifurcation $\xi_{\mathcal{L}\mathcal{R}^2}$ all homoclinic orbits of $\mathcal{O}_{\mathcal{L}^2\mathcal{R}}$ collapse to a single critical homoclinic orbit. After $\xi_{\mathcal{L}\mathcal{R}^2}$ there are no orbits homoclinic to $\mathcal{O}_{\mathcal{L}^2\mathcal{R}}$. Instead, after the bifurcation there are heteroclinic orbits from $\mathcal{O}_{\mathcal{L}^2\mathcal{R}}$ to $\mathcal{O}_{\mathcal{L}\mathcal{R}^2}$. Additionally, when the cycle $\mathcal{O}_{\mathcal{L}\mathcal{R}^2}$ appears there are not only orbits homoclinic to it, but there are also heteroclinic orbits from it to $\mathcal{O}_{\mathcal{L}^2\mathcal{R}}$. Therefore, there are heteroclinic connections between the cycles $\mathcal{O}_{\mathcal{L}^2\mathcal{R}}$ and $\mathcal{O}_{\mathcal{L}\mathcal{R}^2}$, which play the same role as a homoclinic orbit. In this sense we can say that between the bifurcations $\xi_{\mathcal{L}\mathcal{R}^2}$ and $\eta^1_{\mathcal{L}\mathcal{R}^2}$ the cycle is homoclinic due to the presence of a heteroclinic connection between $\mathcal{O}_{\mathcal{L}^2\mathcal{R}}$ and $\mathcal{O}_{\mathcal{L}\mathcal{R}^2}$, although there are no orbits homoclinic to $\mathcal{O}_{\mathcal{L}^2\mathcal{R}}$.

To confirm the existence of a heteroclinic connection between $\mathcal{O}_{\mathcal{L}^2\mathcal{R}}$ and $\mathcal{O}_{\mathcal{L}\mathcal{R}^2}$ we proceed in two steps. First, we confirm the existence of a heteroclinic orbit from $\mathcal{O}_{\mathcal{L}^2\mathcal{R}}$ to $\mathcal{O}_{\mathcal{L}\mathcal{R}^2}$, by using the local unstable set of $\mathcal{O}_{\mathcal{L}^2\mathcal{R}}$ as a target set and calculating the preimages of a point of $\mathcal{O}_{\mathcal{L}\mathcal{R}^2}$. At the parameter value $a_\ell = 0.64$ it follows from Eq. (34) that the target set is given by

$$\mathcal{T} \approx (-1.62639, -1.58594) \cup (-0.02589, 0) \cup (0.99843, 1.01404)$$

Using the algorithm we detect the point

$$q = f_\ell^{-1} \circ f_r^{-1} \circ f_\ell^{-1} \circ f_\ell^{-1} \circ f_r^{-1}\left(x_0^{\mathcal{L}\mathcal{R}^2}\right) \approx 7.83752 \cdot 10^{-4} \in \mathcal{T}$$

This proves the existence of a heteroclinic orbit from $\mathcal{O}_{\mathcal{L}^2\mathcal{R}}$ to $\mathcal{O}_{\mathcal{L}\mathcal{R}^2}$. Similarly, to show the existence of a heteroclinic orbit in the opposite direction, we use as a target set the local unstable set of $\mathcal{O}_{\mathcal{L}\mathcal{R}^2}$ and calculate the preimages of a point of $\mathcal{O}_{\mathcal{L}^2\mathcal{R}}$. At $a_\ell = 0.64$ we get from Eq. (29) the target set

$$\mathcal{T} \approx (-1.58594, -0.98266) \cup (0, 0.23703) \cup (0.38610, 0.99843)$$

and using the algorithm we find the point

$$q' = f_r^{-1} \circ f_\ell^{-1} \circ f_r^{-1}\left(x_0^{\mathcal{L}^2\mathcal{R}}\right) \approx 0.39125 \in \mathcal{T}$$

The homoclinic bifurcation of the cycle $\mathcal{O}_{\mathcal{L}\mathcal{R}^2}$ occurring at $\eta^1_{\mathcal{L}\mathcal{R}^2}$ leads not only to the disappearance of homoclinic orbits to this cycle, but also to the disappearance of heteroclinic orbits from $\mathcal{O}_{\mathcal{L}\mathcal{R}^2}$ to $\mathcal{O}_{\mathcal{L}^2\mathcal{R}}$. Note that heteroclinic orbits from $\mathcal{O}_{\mathcal{L}^2\mathcal{R}}$ to $\mathcal{O}_{\mathcal{L}\mathcal{R}^2}$ do still exist after this bifurcation, as can easily be confirmed by the algorithm discussed above. However, without heteroclinic orbits leading in the opposite direction they do not play any significant role for the dynamics. Therefore, one can say that at the homoclinic bifurcation of the cycle $\mathcal{O}_{\mathcal{L}\mathcal{R}^2}$ occurring at $\eta^1_{\mathcal{L}\mathcal{R}^2}$ the cycle $\mathcal{O}_{\mathcal{L}\mathcal{R}^2}$ becomes non-homoclinic without undergoing a homoclinic bifurcation, but a heteroclinic one.

7. Summary and outlook

In this work we discussed an algorithm which makes it possible to determine the existence of homoclinic and heteroclinic orbits (and hence, heteroclinic connections) of fixed points and cycles in 1D maps. Although the basic idea of the algorithm is straightforward, several optimization steps discussed in this work (in particular, definition of a suitable target set and use of the original function instead of the iterated one) lead to a significant extension of the practical applicability of the algorithm. In particular, as illustrated above, the algorithm can be of assistance for the explanation of complex sequences of homoclinic bifurcations related to repelling cycles.

As a next step, the question arises whether it is possible to apply the algorithm to maps in $\mathbb{R}^n$ with $n > 1$. As the algorithm is based on convergence of orbits in backward time, it can be applied mainly to expanding fixed points or cycles. Still, this task is important as well (due to the same reasons as in 1D), and the algorithm provides a good basis for solving it. Clearly, when dealing with a map in $\mathbb{R}^n$ with $n > 1$, the signature of the inverse functions changes to $f_j^{-1} : \mathbb{R}^n \mapsto \mathbb{R}^n$. Moreover, the crucial point of the implementation is an appropriate data structure for the invariant region $\mathcal{I}$, the target set $\mathcal{T}$, and the domains of the inverse functions $\mathcal{V}_j$, which are now subsets of $\mathbb{R}^n$. However, as all these regions represent the input of the algorithm and do not change during the computations, it is enough to provide for each of these regions a corresponding function with the signature $\mathbb{R}^n \mapsto \{true, false\}$, which determines whether a given point of $\mathbb{R}^n$ belongs to the corresponding region.

Acknowledgments

The work of the first author was supported by the European Community within the scope of the project "Multiple-discontinuity induced bifurcations in theory and applications" (Marie Curie Action of the 7th Framework Programme). The work of the second author was supported by the German Research Foundation within the scope of the project "Organizing centers in discontinuous dynamical systems: bifurcations of higher codimension in theory and applications".

References

[1] Avrutin V, Eckstein B, Schanz M, Schenke B. Bandcount incrementing scenario revisited and floating regions within robust chaos. Math Comput Simul 2014;95:23–38 (Special issue: Discontinuous dynamical systems: theory and numerical methods).
[2] Avrutin V, Gardini L, Schanz M, Sushko I. Bifurcations of chaotic attractors in one-dimensional maps. Int J Bifurcation Chaos 2014;24(8):1440012.
[3] Avrutin V, Schanz M. On the fully developed bandcount adding scenario. Nonlinearity 2008;21:1077–103.
[4] Avrutin V, Sushko I. A gallery of bifurcation scenarios in piecewise smooth 1d maps. In: Bischi G-I, Chiarella C, Sushko I, editors. Global analysis of dynamic models in economics, finance and the social sciences. Springer; 2012. p. 369–95.
[5] Banerjee S, Yorke JA, Grebogi C. Robust chaos. Phys Rev Lett 1998;80:3049–52.
[6] Gardini L. Homoclinic bifurcations in n-dimensional endomorphisms, due to expanding periodic points. Nonlinear Anal Theory Methods Appl 1994;23(8):1039–89.
[7] Gardini L, Cathala JC, Mira C. Contact bifurcations of absorbing and chaotic areas in two-dimensional endomorphisms. In: Forg-Rob W, editor. Iteration theory. World Scientific; 1996. p. 100–11.
[8] Gardini L, Sushko I, Avrutin V, Schanz M. Critical homoclinic orbits lead to snap-back repellers. Chaos Solitons Fract 2011;44:433–49.
[9] Grebogi C, Ott E, Romeiras F, Yorke J. Critical exponents for crisis-induced intermittency. Phys Rev A 1987;36(11):5365.
[10] Grebogi C, Ott E, Yorke JA. Chaotic attractors in crisis. Phys Rev Lett 1982;48:1507–10.
[11] Grebogi C, Ott E, Yorke JA. Crisis: sudden changes in chaotic attractors and transient chaos. Phys D 1983;7:181.
[12] Marotto F. Snap-back repellers imply chaos in R^n. J Math Anal Appl 1978;63:199–223.
[13] Marotto F. On redefining a snap-back repeller. Chaos Solitons Fract 2005;25:25–8.
[14] Mira C, Gardini L, Barugola A, Cathala J-C. Chaotic dynamics in two-dimensional noninvertible maps. World scientific series on nonlinear science, vol. 20. New Jersey: World Scientific; 1996.
[15] Mira C, Narayaninsamy T. On behaviors of two-dimensional endomorphisms: role of the critical curves. Int J Bifurcation Chaos 1993;3(01):187–94.